**Atmospheric
Chemistry
and Physics**

Nocturnal nitrogen oxides at a rural mountain-site in south-western Germany

J. N. Crowley[1], **G. Schuster**[1], **N. Pouvesle**[1], **U. Parchatka**[1], **H. Fischer**[1], **B. Bonn**[2], **H. Bingemer**[2], **and J. Lelieveld**[1]

[1]Max-Planck-Institut für Chemie, Atmospheric Chemistry Dept., Mainz, Germany
[2]Universität Frankfurt, Fachbereich Geowissenschaften, Frankfurt am Main, Germany

Abstract. A new, two-channel instrument for simultaneous NO_3 and N_2O_5 monitoring was used to make the first comprehensive set of nocturnal NO_x measurements (NO, NO_2, NO_3 and N_2O_5) at the Taunus Observatory, a rural mountain site (Kleiner Feldberg) in South-western Germany. In May 2008, NO_3 and N_2O_5 mixing ratios were well above the instrumental detection limit (a few ppt) on all nights of the campaign and were characterised by large variability. The concentrations of NO_3, N_2O_5 and NO_2 were consistent with the equilibrium constant, K_2, defining the rates of formation and thermal dissociation of N_2O_5. A steady-state lifetime analysis is consistent with the loss of nocturnal NO_x being dominated by the reaction of NO_3 with volatile organic compounds in this forested region, with N_2O_5 uptake to aerosols of secondary importance. Analysis of a limited dataset obtained at high relative humidity indicated that the loss of N_2O_5 by reaction with water vapour is less efficient (>factor 3) than derived using laboratory kinetic data. The fraction of NO_x present as NO_3 and N_2O_5 reached ~20% on some nights, with night-time losses of NO_x competing with daytime losses.

1 Introduction

Daytime oxidation processes (e.g. of volatile organic trace gases, VOC) are dominated by the photochemically generated hydroxyl radical (OH), which is present at much reduced levels during the night. At night-time, the nitrate radical, NO_3, is considered the major initiator of oxidation of certain classes of gas-phase organic compounds such as biogenic terpenes and dimethyl sulphide (Wayne et al., 1991).

NO_3 is formed predominantly in the reaction of NO_2 with ozone (Reaction R1) and is converted to N_2O_5 via further reaction with NO_2 (Reaction R2a). Due to the thermal decomposition of N_2O_5 to NO_2 and NO_3 (Reaction R2b), the relative concentrations of NO_3 and N_2O_5 are closely linked (Brown et al., 2003a) and are a strong function of temperature and [NO_2].

$$NO_2 + O_3 \rightarrow NO_3 + O_2 \tag{R1}$$

$$NO_2 + NO_3 + M \rightarrow N_2O_5 + M \tag{R2a}$$

$$N_2O_5 + M \rightarrow NO_2 + NO_3 + M \tag{R2b}$$

As a consequence of its rapid photolysis and reaction with NO (Reaction R4), the NO_3 radical is absent or at significantly reduced concentration during the day and the rapid equilibrium (Reactions R2a, R2b) ensures very low concentrations of N_2O_5 also. Apart from regions impacted by strong anthropogenic NO emissions or very close to the surface where soil emissions of NO are important, NO is rapidly converted to NO_2 via Reaction (R3) at night enabling a build up of NO_3 and N_2O_5. In rural areas NO_2, NO_3 and N_2O_5 are thus the only nocturnal nitrogen oxides apart from long lived, reservoir species such as HNO_3 or PAN.

$$NO + O_3 \rightarrow NO_2 + O_2 \tag{R3}$$

$$NO_3 + NO \rightarrow 2NO_2 \tag{R4}$$

The lifetime of NO_3 is then controlled mainly by its reactions with certain VOCs, whereas N_2O_5 (an acid anhydride) is lost mainly by heterogeneous hydrolysis on aerosol surfaces to result in aqueous phase nitrate formation:

$$NO_3 + VOC \rightarrow products \tag{R5}$$

$$N_2O_5 + aerosol \rightarrow nitrate \tag{R6}$$

Close to ground level, dry deposition could also be important for both NO_3 and N_2O_5.

The sequential oxidation of NO to NO_2 to NO_3 to N_2O_5 and finally to particulate nitrate thus represents a change in the partitioning of nitrogen oxides between the NO_x ($NO+NO_2$) and NO_z families, where NO_z is the sum of all nitrogen oxides (NO_y) minus NO_x. Note that N_2O_5 contributes twice to NO_y as it contains two N-atoms. The heterogeneous loss of N_2O_5 or NO_3 also modifies the partitioning of NO_y between the gas and particulate phases. Both the modification of the NO_x/NO_y ratio and the oxidation of VOCs by NO_3 impact daytime photochemical rates.

Given sufficient time, a stationary state is reached for NO_3 at night in which its production (the rate of which is given by $k_1[NO_2][O_3]$) is approximately balanced by the sum of direct losses and indirect loss via conversion to N_2O_5 and subsequent heterogeneous removal. The turnover lifetime of NO_3 in steady state, $\tau_{ss}(NO_3)$, which is defined as the inverse of the sum of the direct and indirect loss frequencies ($\tau_{ss}(NO_3)=1/(f_{dir}(NO_3)+f_{indir}(NO_3))$), is given by:

$$\tau_{ss}(NO_3)=\frac{[NO_3]}{k_1[NO_2]\cdot[O_3]} \qquad (1)$$

In the absence of both light and NO the direct losses of NO_3 are dominated by reactions with organic trace gases (Reaction R5) so that, to a good approximation, $f_{dir}(NO_3)=\Sigma(k_i[VOC]_i)$ where k_i is the rate coefficient for reaction of NO_3 with a specific VOC of concentration [VOC]. The rate of indirect loss of NO_3 via its conversion to N_2O_5 depends on the equilibrium constant (K_2) that defines the relative concentration of NO_3 and N_2O_5 for any given temperature and amount of NO_2.

$$K_2=\frac{[N_2O_5]}{[NO_2]\cdot[NO_3]}=\frac{k_2}{k_{-2}} \qquad (2)$$

The frequency of indirect loss of NO_3 is thus given by $f_{indir}(NO_3)=K_2[NO_2](f_{het}+f_{homo})$. Where f_{het} is the loss frequency for N_2O_5 due to irreversible, heterogeneous uptake to aerosol surfaces and f_{homo} is the loss frequency of N_2O_5 due to gas-phase reaction with water vapour. Combining the definitions of $f_{dir}(NO_3)$ and $f_{indir}(NO_3)$ with Eq. (1) and ignoring loss of NO_3 or N_2O_5 by dry deposition, we derive (Geyer et al., 2001; Aldener et al., 2006):

$$\tau_{ss}(NO_3) \approx \frac{1}{f_{dir}(NO_3)+f_{indir}(NO_3)}$$
$$\approx \frac{1}{f_{dir}(NO_3)+K_2[NO_2](f_{het}+f_{homo})} \qquad (3)$$

For aerosol particles of diameter less than ~1 micron, f_{het} is given by:

$$f_{het} \approx \frac{\gamma\cdot\bar{c}\cdot A}{4} \qquad (4)$$

where A is the aerosol surface area density ($cm^2\,cm^{-3}$), $\bar{c}$ is the mean molecular velocity of N_2O_5 ($23\,500\,cm\,s^{-1}$ at

280 K) and γ is the dimensionless uptake coefficient. The available kinetic data (Atkinson, 2004) indicates a gas-phase reaction between N_2O_5 and H_2O which contains terms both linear and quadratic in H_2O concentration:

$$N_2O_5+H_2O \rightarrow 2HNO_3 \qquad (R7a)$$

$$N_2O_5+2H_2O \rightarrow 2HNO_3+H_2O \qquad (R7b)$$
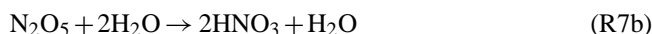
with $k_{7a}=2.5\times10^{-22}$ cm^3 molecule^{-1} s^{-1} and $k_{7b}=1.8\times10^{-39}$ [H_2O] cm^3 molecule^{-1} s^{-1}. As [H_2O]$\gg$ [N_2O_5], pseudo first-order kinetics are applicable so that

$$f_{homo}=k_{7a}[H_2O]+k_{7b}[H_2O]^2 \qquad (5)$$

with the H_2O concentration in units of molecule cm^{-3}. Recent field measurements (Brown et al., 2006, 2009) have cast doubt on the accuracy of the laboratory studies, suggesting that the reaction proceeds significantly slower (see later).

The relative importance of direct and indirect loss mechanisms for NO_3 depends on several factors including the concentrations of NO_2 and VOCs, the available surface area (A) and the temperature, which strongly influences K_2, emission rates of biogenic VOCs (Geyer and Platt, 2002) and available H_2O-vapour. For this reason, the direct and indirect loss mechanisms can show large regional and seasonal dependencies, with NO_3 lifetimes close to the surface varying from minutes in areas impacted by anthropogenic or biogenic emissions to hours in remote regions (Heintz et al., 1996; Allan et al., 2000).

In this paper we describe the first deployment of a new, two-channel optical cavity based instrument for detection of NO_3 and N_2O_5, and also the first measurements of NO_3 or N_2O_5 at the Taunus Observatory, a rural mountain site in South-western Germany. Ancillary measurements of NO, NO_2, O_3 and aerosol surface area enabled us to calculate NO_3 and N_2O_5 lifetimes and assess some aspects of nocturnal chemistry at this site.

2 Experimental

2.1 Site description

The measurements were made at the Taunus Observatory, located at 50°13′25″ N, 8°26′56″ E and 825 m above sea level at the summit of the "Kleiner Feldberg" a mountain in the Taunus range in South-western Germany (Fig. 1). The area directly around the observatory is mainly coniferous forest (predominantly spruce). The hill top itself (50 m in radius) has been cleared of trees for meteorological measurements several times, the last time about half a century ago and only a couple of willows and some birch trees remain between the cleared area and the spruce trees. The direct vicinity of the measurement containers is covered by shrubs and blueberry plants. Because of its elevation the station is known for its quite remote character for central Germany with a
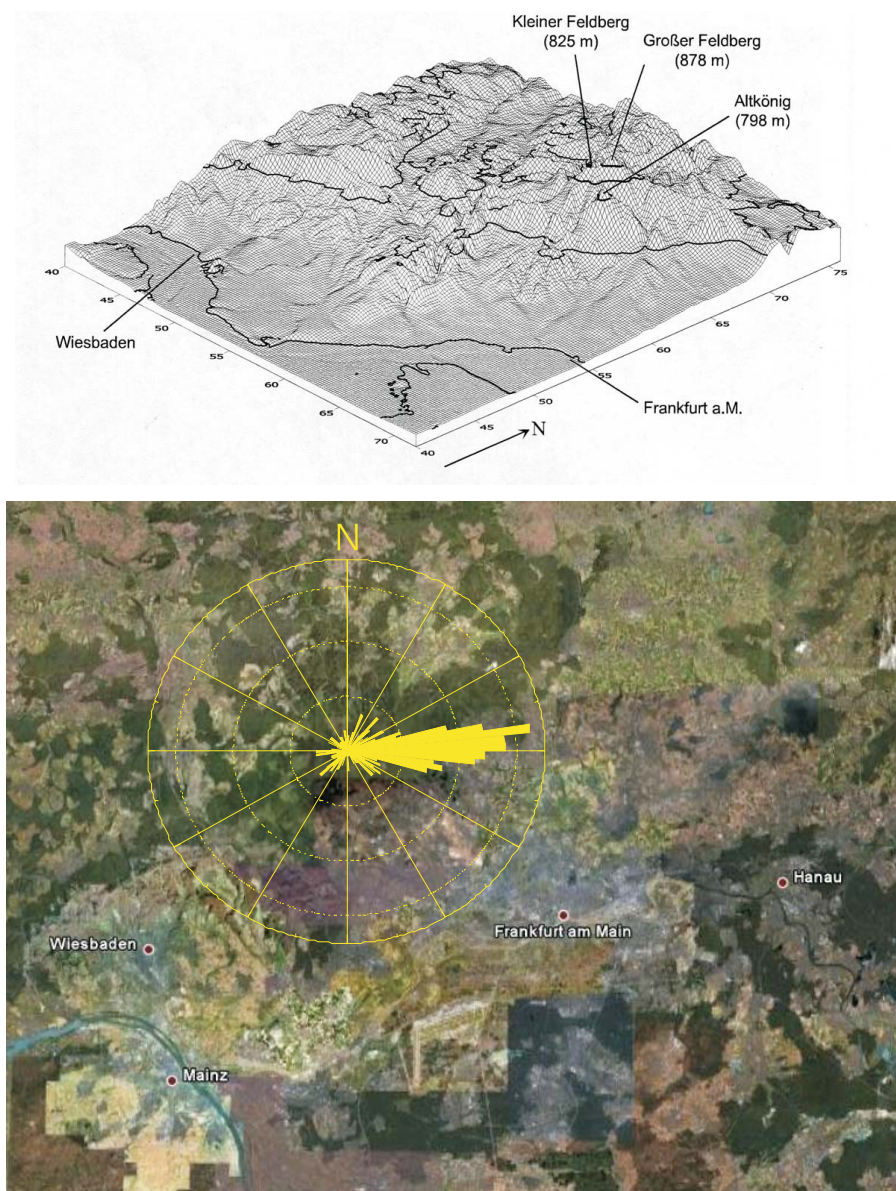
Fig. 1. Upper: Topographic map indicating the location of the Taunus Observatory at the summit of the Kleiner Feldberg (from PhD thesis of G. M. Handisides). Lower: Relation of site to local cites indicating predominant wind directions during the campaign.

few main roads and some small towns within 5 km. The observatory is impacted by pollution from the heavily populated Rhein-Main area (pop. ~2 million) including a dense motorway system and large cities such as Frankfurt (pop. ~700 000, 30 km SE), Wiesbaden (pop. ~300 000, 20 km SW) and Mainz (pop. ~200 000, 25 km SSW). The area 50–100 km north of Kleiner Feldberg is lightly populated and devoid of major industry. Wind flow patterns are influenced by the presence of two similar sized mountains: Altkönig (798 m) and Großer Feldberg (878 m) in the direct vicinity (2.7 km and 1.3 km distant, respectively). Previous measurements have shown that highest CO levels at the Taunus Ob-

servatory were associated with Easterly winds containing air from the Frankfurt region which have been channelled between the Großer Feldberg and Altkönig mountains (Wetter, 1998) with highest levels of O_3 arriving with wind from the east to southeast during warm, sunny periods (Handisides, 2001). As well as the Taunus Observatory, the meteorological garden of the German weather service (DWD) and the measurement container of the State of Hessen environmental agency (HLUG) are also located at the summit of the Kleiner Feldberg.
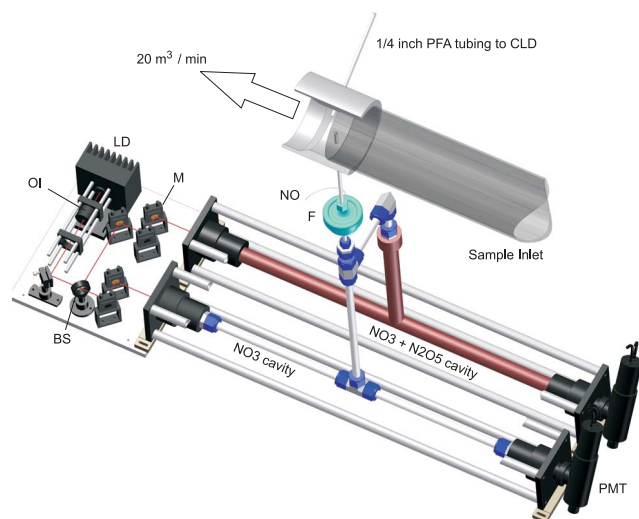
Fig. 2. Two-channel NO_3/N_2O_5 instrument. The sample inlet was a 1.4 m long Teflon coated glass tube (ID 104 mm). Gas was sampled from the centre of the tube to the NO_3/N_2O_5 and $NO/NO_2/O_3$ instruments and exits close to the cavity mirrors as described in detail by Schuster et al. (2009). The NO_3 cavity was made of PFA tubing and fittings (thermal insulation not shown), the $N_2O_5+NO_3$ cavity was made of Teflon (FEP) coated glass (heating elements and insulation not shown). NO=NO addition point for NO_3 titration. F=PFA filter folder with 2 μm PTFE filter. OI=optical isolator. BS=beam splitter (70% for NO_3 cavity, 30% for $NO_3+N_2O_5$ channel). PMT=housing with photomultiplier and interference filter. M=Aluminium coated mirror. LD=Laser diode in temperature controlled housing. CLD=chemiluminescence instrument for NO, NO_2 and O_3.

2.2 Instrumentation

The instruments were located in the upper container of a two-container tower, with the inlet ∼4.5 m above the ground. In order to avoid trace gas losses (especially of NO_3) the inlet was constructed from a 1.4 m long, glass tube of internal diameter 10.4 cm, which was internally coated with a thin film of Teflon (FEP 100a). An industrial fan attached to the exit of the glass tube maintained a flow (at circa 700 Torr) of ∼20 m^3 min^{-1} through the tube, resulting in residence times of ∼0.1 s to the sampling line. 18 L min^{-1} air was sampled (at 90° to the main flow) from the centre of the large diameter tube via a short piece of $^1/_4''$ PFA-Teflon tubing (∼15 cm) and a 2 μm pore Teflon filter to the NO_3/N_2O_5 instrument. An ∼4 m length of $^1/_4''$ PFA-Teflon tubing, sampling at ∼3 L/min from the centre of the inlet, transferred air to the $NO/NO_2/O_3$ detector (see below). Physical characterisation of the aerosol size distribution and aerosol number concentration was performed via inlets from the same container used for NO_3 and N_2O_5 measurements. Smaller particles were sampled through a 1 m long Tygon tube, which was mounted horizontally straight out of the container window in order to keep sampling losses as small as possible.

Larger particles were sampled via a vertical glass tube extending above the roof of the upper container. This inlet was covered by a cap to prevent rain from entering.

2.2.1 NO_3 and N_2O_5 measurements

NO_3 and N_2O_5 mixing ratios were measured using a two-channel, off axis cavity-ring-down system (OA-CRD). A single channel prototype of this device was described recently (Schuster et al., 2009) and took part in a major NO_3/N_2O_5 inter-comparison at an environmental chamber in 2007 (Apodaca et al., 2009; Dorn et al., 2010). The major modification of the device for the present campaign was the introduction of a second cavity to enable simultaneous measurement of NO_3 and N_2O_5. This is the first implementation of the two-channel device in the field and it is therefore described in some detail.

The instrument and inlet configuration is shown in Fig. 2. The NO_3 cavity (PFA tubing, resonator length 70 cm, volume 79 cm^3) was operated close to ambient temperature, whereas the summed concentration of $NO_3+N_2O_5$ was measured in a Teflon coated Pyrex cavity (resonator length 70 cm, volume 165 cm^3) heated to 80 °C. The heated cavity was located behind a ∼20 cm section of Teflon coated glass tubing heated to 85 °C to quantitatively convert N_2O_5 to NO_3. Laboratory tests showed that, at the given flow rate and residence time in the converter, this temperature was sufficient to quantitatively dissociate N_2O_5. Note that the cavity temperature was cooler than in our prototype device, (Schuster et al., 2009) which was operated at 95 °C. The flow rates through the cavities were 10 L(std) min^{-1} (NO_3) and 8 L(std) min^{-1} ($N_2O_5+NO_3$), resulting in residence times of ∼0.4 s and 0.8 s, respectively.

The light source used was a ∼100 mW laser diode operated at 662 nm, close to the peak of the NO_3 absorption spectrum. The laser current was modulated to broaden the laser-spectral bandwidth and improve the signal/noise ratio of the cavity emission, without loss of overlap with the broad NO_3 spectrum (Schuster et al., 2009). Light exiting the cavity was filtered by a 662 nm interference filter prior to detection by a PMT. The pre-amplified PMT signal was digitised and averaged with a 10 MHz, 12 bit USB scope (Picoscope 3424) which was triggered at the laser modulation frequency of 100 Hz. Typically 256 ring-down events were recorded to result in a time resolution of ∼3 s. The cavity loss due to absorption at 662 nm was calculated from the change in ring-down constant in the presence of an absorber and converted to a concentration of NO_3 using the effective cross section of NO_3 at the experimental temperature and the established relation (Berden et al., 2000; Mazurenka et al., 2005)

$$[NO_3] = \frac{\Delta k_{rd} L}{\sigma_{NO3} cd} \tag{6}$$

where [NO_3] is the concentration of NO_3 (molecule cm^{-3}), k_{rd} is the ring-down constant (a first-order rate coefficient

with units of s^{-1}), Δk_{rd} is the difference in the ring-down decay constant with and without NO$_3$, L is the distance between the cavity mirrors (70 cm), d is the length of the cavity which is filled with absorber, σ_{NO3} is the effective absorption cross section of NO$_3$ and c is the speed of light $\sim 2.998 \times 10^{10}$ cm s^{-1}). Temperature dependent values of σ_{NO3} have been determined by Yokelson et al. (1994) and Osthoff et al. (2007). The parameterisations of Orphal et al. (2003) and Osthoff et al. (2007) both give a value of 1.77×10^{-17} cm^2 molecule^{-1} at the peak of the 662 nm band at 80 °C. This value was convoluted with the laser emission profile to obtain effective cross sections as described previously (Schuster et al., 2009).

The ring-down constant in the absence of NO$_3$ was derived by adding $\sim 10^{12}$ molecule cm^{-3} of NO (8 sccm of a 100 ppm mixture of NO in N$_2$) to the air above the filter every 100 s for a period of ~ 20 s (duty cycle of 80%). Slight drifts in the ring-down constant over the course of an hour were then removed from the dataset by fitting a polynomial to the ~ 36 titration points obtained in the presence of NO. Typically, for the NO$_3$ channel the standard deviation in the fit was ~ 1 ppt, whereas for the sum channel it was ~ 2.5 ppt.

By variation of the mirror purge gas flow whilst monitoring the ring-down signal due to a constant flow of NO$_2$ into the cavity (NO$_2$ also absorbs at 662 nm), we were able to calculate a value of L/d of 1.01 ± 0.03. Note that the ring-down time constant, τ, is equal to $1/k_{rd}$ and for a cavity free of absorbing species was typically close to 80 µs, indicating an effective optical path length of ~ 25 km.

Loss of NO$_3$ to the filter was determined in the laboratory as described previously (Schuster et al., 2009) by flowing NO$_3$ or N$_2$O$_5$ (generated in the reaction of NO$_2$ with O$_3$) into the cavities with and without a filter in place. Repeated tests resulted in a clean filter transmission of $90 \pm 3\%$ for NO$_3$ and $98 \pm 2\%$ for N$_2$O$_5$. During the campaign, the filter was usually changed at 1 h intervals to prevent significant build up of a reactive surface. We show later that leaving the filter for two hours did on one occasion result in loss of NO$_3$ transmission (but not N$_2$O$_5$).

The data also required correction for loss of NO$_3$ during transport through the cavities. This was achieved by carrying out pre- and post-campaign experiments in the laboratory in which a 11 SLM flow of air containing stable concentrations of N$_2$O$_5$ and NO$_3$ was passed through both cavities. By varying the relative flow rate through each cavity whilst maintaining the total flow and thus NO$_3$/N$_2$O$_5$ concentration, the residence time of gas in each cavity was varied. As described previously (Schuster et al., 2009) an exponential dependence of the NO$_3$ signal on residence time was observed, allowing loss terms of 0.25 ± 0.05 s^{-1} (cold cavity) and 0.11 ± 0.05 s^{-1} (hot cavity) to be derived. Based on known cavity residence times when sampling from the atmosphere, the corrections to the field data for cavity losses were calculated as $11 \pm 2\%$ for both channels.

Other corrections that can be applied to the data result from chemistry within the cavities. The addition of NO to titrate NO$_3$ whilst measuring the ring-down constant in the absence of NO$_3$ (chemical zero) disturbs the equilibrium between NO$_3$ and N$_2$O$_5$, and leads to N$_2$O$_5$ dissociation to NO$_3$. The magnitude of this effect (essentially an error in the determination of the chemical zero) can be estimated in a steady state analysis from the amount of N$_2$O$_5$, the cavity temperature and the NO added as:

$$[NO_3]_{extra} = \frac{k_{-2}[N_2O_5]}{k_4[NO]} \tag{7}$$

At a typical cavity temperature of 292 K, k_{-2} is ~ 0.02 s^{-1} and k_4 is 3.6×10^{-11} cm^3 molecule^{-1} s^{-1}. The extra NO$_3$ formed in this process is ~ 0.2 ppt at N$_2$O$_5$ mixing ratios of 200 ppt. As such N$_2$O$_5$ mixing ratios were always associated with NO$_3$ mixing ratios of 20 ppt or more, this represents an insignificant effect (sub percent).

In addition to titrating NO$_3$, the addition of NO can lead to NO$_2$ formation via its reaction with ambient O$_3$. As both NO$_2$ and O$_3$ absorb weakly at 662 nm, (cross sections are $\sim 2 \times 10^{-21}$ cm^2 molecule^{-1} for NO$_2$ and 1×10^{-21} cm^2 molecule^{-1} for O$_3$) this can also have an impact on the retrieved chemical zero. The amount of NO$_2$ formed during titration, $\delta[NO_2]$, may be approximated by:

$$\delta[NO_2] = [O_3]\left\{1 - \exp^{(-k_3 \cdot [NO] \cdot t)}\right\} \tag{8}$$

where t is the cavity residence time (0.88 s in the N$_2$O$_5$+NO$_3$ cavity and 0.44 s in the NO$_3$ cavity). k_3 is equal to 4.3×10^{-14} cm^3 molecule^{-1} s^{-1} at 80 °C (hot cavity) and 1.8×10^{-14} cm^3 molecule^{-1} s^{-1} at ~ 290 K (cold cavity). We assume O$_3$ is 80 ppb (the largest value measured in the campaign). For the hot cavity $\delta NO_2 = 3$ ppb, and for the cold cavity just 0.6 ppb. Given the values of the NO$_2$ and O$_3$ cross sections listed above, this represents an error of just 0.15 ppt equivalents (N$_2$O$_5$+NO$_3$ cavity) and 0.03 ppt (NO$_3$ cavity) which are much lower than noise levels and fluctuations in the chemical zero.

Although the cold cavity was heavily insulated, we measured temperatures within the cavity that were ~ 4–5 °C warmer than ambient. A warming of the cavity compared to ambient air can potentially impact on the NO$_3$ measurement as a new equilibrium between N$_2$O$_5$ and NO$_3$ may be established, leading to an overestimation of the true NO$_3$ concentration and also the NO$_3$/N$_2$O$_5$ ratio. As a first approximation, an upper limit to the size of this effect can be estimated from the concentration of N$_2$O$_5$, the known dissociation rate constant (k_{-2}) at the temperature of the cavity and the average residence time (t) of N$_2$O$_5$ in the cavity.

$$\delta[NO_3] = [N_2O_5]_0 (1 - \exp(-k_{-2}t)) \tag{9}$$

At 290 K (typical ambient temperatures were 280–285 K), the thermal dissociation rate constant for N$_2$O$_5$ is 1.4×10^{-2} s^{-1}. The average residence time is taken as the

time for gas to be transported half way between the T-piece connector to the centre of the cavity and the exit and is $\sim$0.26 s. This estimation of the residence time takes into account the fact that we "integrate" the NO_3 concentration over the entire cavity length. These values of k_{-2} and t result in $\sim$0.4% conversion of the N_2O_5 to NO_3, which represents a maximum correction of 1.6 ppt for NO_3 when N_2O_5 was close to 400 ppt (the largest values measured in the campaign). This calculation does not take into account the fact that the formation and loss rates of N_2O_5 are not de-coupled at this temperature. As typical vales of NO_2 were 1–2 ppb ($\sim$2–4$\times$10^{10} molecule cm^{-3}) the instantaneous first-order constant for N_2O_5 formation (k_2 [NO_2]) is 2.5–5$\times$10^{-2} s^{-1}, i.e. similar to its thermal dissociation rate constant. More accurate correction factors were thus obtained by numerical simulation (Curtis and Sweetenham, 1987) of the effect of a 5 °C temperature jump in $NO_2/NO_3/N_2O_5$ mixtures at equilibrium and at similar concentrations to those measured in the campaign. The results showed that the maximum change in NO_3 or the NO_3/N_2O_5 ratio was $\sim$1–1.5%. This effect was considered too small to warrant correction to the data, though it is worth noting that long cavity residence times and larger temperature increases between ambient and cavity will result in significant systematic overestimation of NO_3 under some conditions.

The random noise limited detection limits (3 s integration per datapoint) were 1–2 ppt (NO_3) and 4–5 ppt (N_2O_5). As summarised by Schuster et al. (2009), when considering the above and taking into account estimated errors in the NO_3 cross section at both cavity temperatures we estimate the uncertainty (2σ) to be $\pm$15% for NO_3 and at least 2 ppt. For the N_2O_5 channel these values are $\pm$15% and at least 3 ppt.

2.2.2 NO, NO_2 and O_3 measurements

The measurements of NO, NO_2 and O_3 were based on the chemiluminescence of the reaction between NO and O_3 (Fontijn et al., 1970). The instrument is a modified commercial Chemiluminescence Detector (CLD 790 SR) originally manufactured by ECO Physics (Duernten, Switzerland). The original instrument housed two CLD channels, that were used for the detection of NO and NO_2. The quantitative detection of NO_2 is based on its photolytic conversion (Blue Light Converter, Droplet Measurement Technologies, Boulder, Co, USA) to NO, which was subsequently detected in the CLD (Kley and McFarland, 1980). A third channel was added for the measurements of O_3 following the design described by Ridley et al. (1992). In the present study data were obtained at a time resolution of 2 s.

In-field calibrations for NO were made on a regular basis by adding a secondary standard (2 ppmv NO in N_2, Air Liquide, Germany) diluted by zero air to a mixing ratio of approximately 2 ppbv. The zero air, that was also used for regular background measurements, was produced from synthetic air (Air Liquide, Germany), that was additionally filtered through a catalytic air purifier (Pt/Pd) and charcoal and "Purafil" ($KMnO_4/Al_2O_3$) cartridges. The secondary NO standard used in the field was traced to a primary standard (NIST, USA). The efficiency of the Blue Light Converter for NO_2 measurements was determined by gas phase titration of NO (from the secondary standard) using an excess of O_3. This procedure yielded a conversion efficiency of (46.6$\pm$2)% over the campaign. The ozone channel was calibrated using a commercial O_3 calibrator (model TE49C, Thermo Instruments, Germany).

The detection limits (based on reproducibility of zero measurements) for the NO and NO_2 measurements were 10 ppt and 80 ppt, respectively for an integration period of 2 s. The total uncertainties (2σ) for the measurements of NO, NO_2, and O_3 were determined to be 10%, 10% and 5%, respectively, based on the reproducibility of in-field background measurements, calibrations, the uncertainties of the standards and the conversion efficiency of the photolytic converter.

2.2.3 Particle measurements

Aerosol number and size distribution was monitored using a scanning mobility particle sizer (TSI 3936), consisting of an electrostatic classifier with a ^{80}Kr source for particle equilibrium charging and a long differential mobility analyser (TSI 3081) with a condensation particle counter (TSI 3025A) for particle detection. The sheath flow inside the electrostatic classifier was set to 6 L min^{-1} and the sample flow of the ultra fine particle counter was set to its maximum value of 1.5 L min^{-1} (high flow). This set-up allowed particle detection within the size range between 9.8 and $\sim$300 nm in diameter. Each size distribution measurement took 135 s, i.e. 120 s for up scan and 15 s for down scan. Four consecutive measurements were averaged afterwards to obtain a smooth result with a time resolution of ten minutes. In the absence of information regarding composition, a particle density of 1.2 g cm^{-3} was assumed. Larger particles with a diameter between 360 nm and 19 μm were detected occasionally by an aerosol particle sizer (APS, TSI 3321) using a sampling flow rate of 1 L min^{-1}. Typical night-time particle concentrations as measured by the SMPS were 2000–5000 particle cm^{-3} with a bi-modal distribution (maxima at $\sim$35 and 120 nm) with most surface area (typically 10^{-6} cm^2 cm^{-3}) contained in particles of radius $\sim$200–250 nm. The APS particle measurements only functioned sporadically and revealed low concentrations of coarse particles (10–20 particle cm^{-3}, with a mean diameter $\sim$600 nm). The APS measurements indicate that particles measured by the SMPS account for at least 65% of the total aerosol surface area and generally close to 80%.
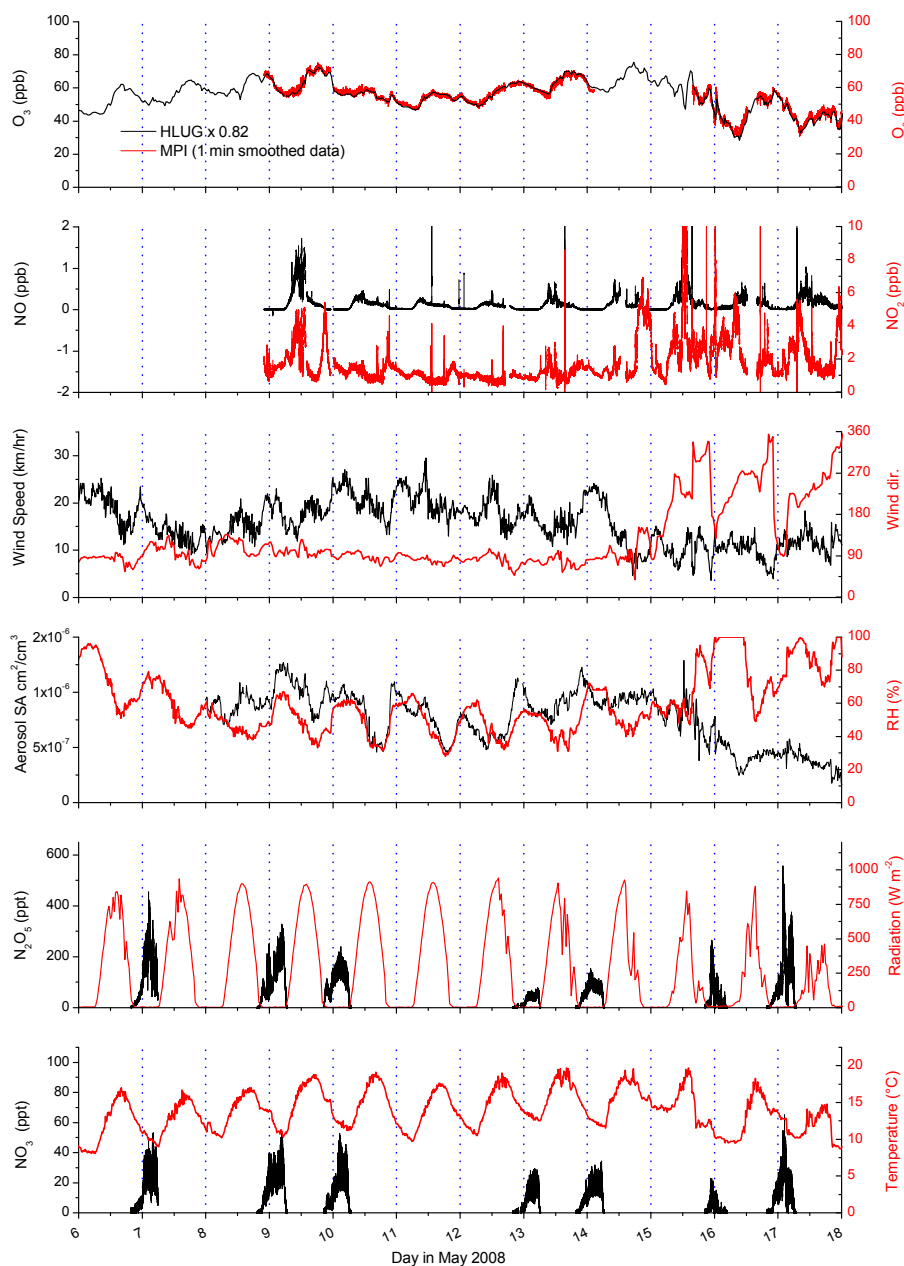
Fig. 3. Trace gas and meteorological overview. Temperature, wind speed and relative humidity were taken measured by the German weather service. Global radiation and wind direction were measured by the Hessen environmental agency (HLUG) who also monitored O_3. The HLUG O_3 values have been scaled by a factor 0.82 to bring them into line with the MPI measurements.

2.2.4 Meteorological data

Atmospheric pressure and temperature, wind direction/speed and relative humidity were available as 10 min averaged data from the German weather service station (DWD), located ∼20 m away from the container. Global radiation was available from the local environmental agency station (HLUG) as 30 min averaged data. These measurements were also located just a few metres away. The HLUG also provided O_3

measurements (30 min averages) using a UV-absorption instrument (API 400).

3 Observations and analysis

The measurements were carried out in May 2008, with almost complete coverage for NO and NO_2 from the 9th until the 20th. O_3 was measured over the same period, but with a break for instrument repair between the 14th and 15th. The
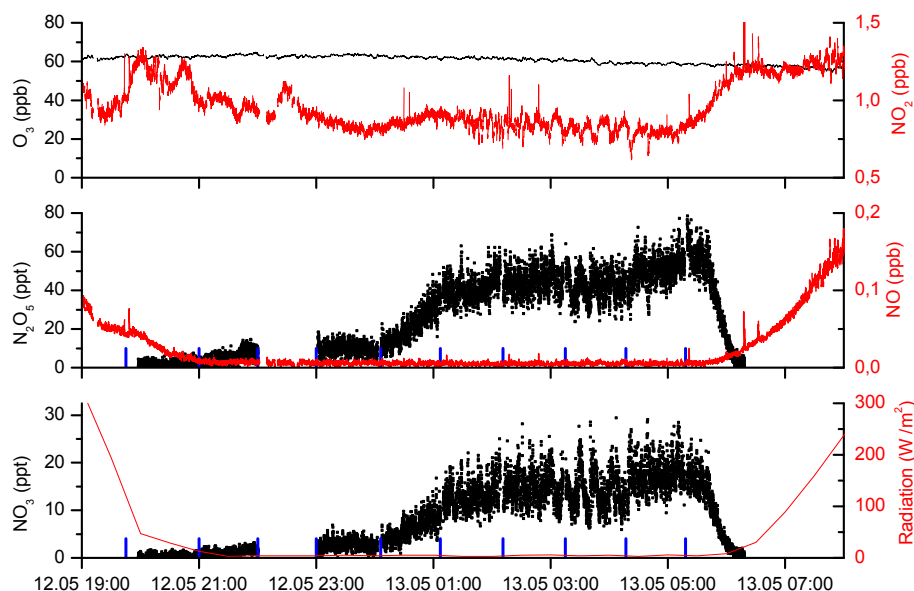
Fig. 4. Data from 12th–13th as exemplary night-time dataset. Great variability in the NO$_3$ and N$_2$O$_5$ mixing ratios is apparent. The approximate time of local sunrise and sunset may be obtained from the half-hourly measurements of global radiation at the site.

NO$_3$/N$_2$O$_5$ instrument was operated on one night prior to and 6 nights within this period. The complete trace gas and meteorological data set is displayed in Fig. 3. NO$_3$/N$_2$O$_5$ measurements typically started just before local sunset and stopped after the signals had returned to baseline levels following sunrise. The early part of the campaign (up to 15 May) was characterised by easterly winds (12–25 km h^{-1}) cloud-free skies and daytime maximum temperatures up to 18 °C. Temperatures at night generally sunk to ∼9–12 °C with relative humidities of 30–45% and no precipitation. After 15 May, the wind direction was more variable with components from the Southwest bringing clouds and rain. NO$_2$ was present at concentrations of typically between 1 and 2 ppb at night, with excursions up to 4 ppb. Daytime mixing ratios were generally less than 10 ppb. O$_3$ was present at levels between 30 and 75 ppb, with maximum mixing ratios of ∼55–75 ppb encountered in the late afternoon, which usually decreased steadily (by 10–20 ppb) during the night. The HLUG O$_3$ mixing ratios have been multiplied by a factor 0.82 to bring them into line with the MPI measurements, which are considered to be more reliable due to frequent calibration.

The high levels of night-time O$_3$ ensured that NO levels were low and usually close to the instrumental detection limit. The conditions were therefore conducive for NO$_3$ chemistry (sufficient NO$_x$ and O$_3$ to drive formation and no NO) and both NO$_3$ and N$_2$O$_5$ were detected on all nights in which the instrument was operated, with maximum mixing ratios of ∼500 ppt and 60 ppt observed for N$_2$O$_5$ and NO$_3$, respectively. A more detailed view is given in Fig. 4, which displays data from one night only (12–13 May). On

this night, NO$_3$ and N$_2$O$_5$ mixing ratios increased above the detection limit shortly after local sunset (at ∼21:00) when both photolysis and NO levels were sufficiently reduced. The lifetime of NO in the presence of ∼60 ppb of O$_3$ is only about 1 min, so that the slow decrease in NO after 19:00 simply reflects the decrease in light intensity and the decreasing photolysis rate of NO$_2$. Maximum values of ∼25 and 70 ppt were reached by NO$_3$ and N$_2$O$_5$, respectively, both displaying great temporal variability, with fluctuations of 15–20 ppt (i.e. up to 50% signal modulation) in one minute (see Fig. S1 of the supplementary information (http://www.atmos-chem-phys.net/10/2795/2010/ acp-10-2795-2010-supplement.pdf) for an example). The short term variability (minutes) of NO$_3$ and N$_2$O$_5$ is typical of a ground site (Brown et al., 2003b). A major contributor to the variability is expected to be sampling of air masses that originate from different altitudes and which have experienced variable rates of loss to both gas-phase reactions and reactions with surfaces including vegetation and architecture between the emission region and the measurement site.

On a slightly longer time scale (10–15 min) there is evidence for variability driven by fluctuations in the NO$_2$ mixing ratio (e.g. between ∼3 a.m. and 5 a.m. on the 13th) which, together with O$_3$, defines the production rate of NO$_3$ and N$_2$O$_5$. At sunrise (∼05:30 local time) both NO$_3$ and N$_2$O$_5$ are rapidly depleted as J_{NO_3} increases. The direct photolysis of NO$_3$ depletes N$_2$O$_5$ via the equilibrium (R2a, R2b) and also releases NO to further remove NO$_3$. NO is also generated in the photolysis of NO$_2$ at roughly the same time, and both NO$_3$ and N$_2$O$_5$ return to below detection limit within 1 h. During this period, NO$_2$ and NO
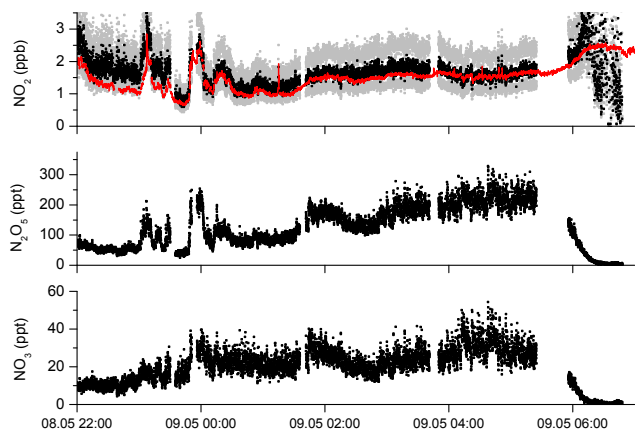
Fig. 5. Measured mixing ratios of NO_2, (upper panel, red line) NO_3 (lower panel) and N_2O_5 (centre). The calculated NO_2 mixing ratios (black line in upper panel with grey error bounds) used evaluated, temperature dependent values of K_2 (Sander et al., 2003).

are observed to increase by 450 ppt and 20 ppt, respectively. The amount of NO_2 released from the degradation of NO_3 and N_2O_5 can be estimated as $2\times[N_2O_5]+[NO_3]$, which, for the data in Fig. 4, amounts to $\sim$140 ppt. This accounts for only $\sim$30% of the total increase in NO_x directly after sunrise. The extra NO_x observed cannot be from degradation of the expected major long lived reservoir species (e.g. HNO_3 and PAN). HONO photolysis may however play a role. Assuming 300 ppt HONO at dawn and an approximate, average value of J-HONO $\sim$1$\times10^{-4}$ s^{-1} (Kraus and Hofzumahaus, 1998) over a 40 min period would result in the release of $\sim$70 ppt of NO. A further possibility is upslope winds (caused by warming of the easterly side of the mountain as the sun rose) bringing fresh NO_x to the site. On one morning (10 May) an excess release of NO_x was not observed, and the generated amounts of NO and NO_2 agreed with that released from NO_3 and N_2O_5. As 10 May 2008 was a Saturday, this may indicate a weekend effect, with upslope winds bringing less locally emitted pollution from early morning commuter traffic.

The blue, vertical lines indicate at which times the Teflon filter was changed. Filter changing was conducted manually, and took $\sim$1–2 min. On this night, there was no evidence for loss of N_2O_5 or NO_3 on the filter, which would have been observable as an increase in the NO_3 or N_2O_5 signal directly after filter changing.

3.1 Equilibrium between NO_2, NO_3 and N_2O_5

According to Reactions (R2a) and (R2b), the relative concentrations of NO_3 and N_2O_5 should be controlled by the temperature dependent equilibrium constant (K_2) and the concentration of NO_2. The time for a chemical system to relax to equilibrium is the sum of the inverse forward and back rate constants, i.e., with NO_2 in large excess over NO_3:
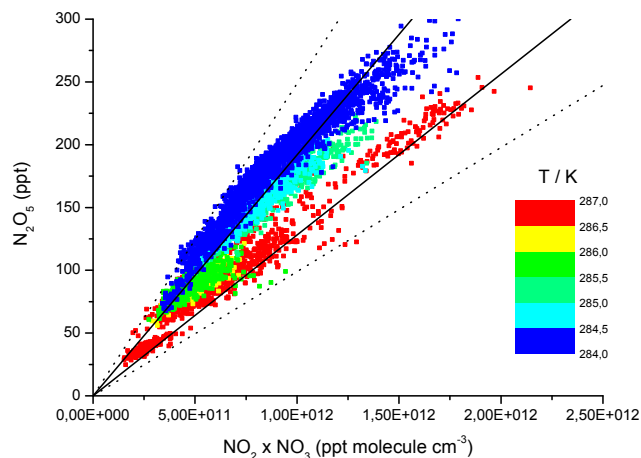
Fig. 6. Determination of the equilibrium constant, K_2. The NO_2, N_2O_5 and NO_3 data used were gathered over an $\sim$3 h period (01:00 to 03:00) on 9 May when the NO_3 level was above 7 ppt. The solid black lines represent the expected slopes (calculated using literature values for K_2) at the extremes of the small temperature range covered, and should therefore encompass all the data. The dotted black lines use the values of K_2 at the outer bounds of the recommended uncertainty in this parameter.

$$\tau_{eq} = \frac{1}{k_2[NO_2]+k_{-2}} \quad (10)$$

At pressures close to 1 bar, the rate constant for the forward reaction (k_2) is circa 10^{-12} cm^3 molecule^{-1} s^{-1}, which when combined with typical NO_2 concentrations of 1.5 ppb ($\sim$4$\times10^{10}$ molecule cm^{-3}), gives a first-order N_2O_5 formation rate constant of 0.04 s^{-1}. The thermal dissociation rate constant for N_2O_5 (k_{-2}) is 0.0064 s^{-1} at the average nighttime temperature of 11$\pm$1.5 °C. This results in a relaxation time to thermal equilibrium of $\sim$100 s and implies that, in the absence of very local sources or sinks of NO_3 or N_2O_5, these species should be in thermal equilibrium. Qualitative confirmation of this could be observed during measurements as even rapid changes in NO_3 and N_2O_5 (see discussion of variability above) closely tracked each other.

Whether equilibrium was acquired could be tested by making a point-by-point comparison of the measured NO_2 mixing ratio (interpolated onto the same time grid as the NO_3/N_2O_5 data) with that calculated from the NO_3 and N_2O_5 observations, the temperature and the literature value for K_2 (T), which is recommended as $K_2=3.0\times10^{-27}\exp(10\,990/T)$ (Sander et al., 2006). The results are shown for the night 8–9 June in Fig. 5. As data filter, only NO_3 mixing ratios greater than 7 ppt were considered. The black data points in the upper panel of Fig. 5 are the calculated NO_2 mixing ratios (NO_2-calc). The grey data points were calculated using the upper and lower bounds of the propagated overall uncertainty in NO_2-calc, which arises from uncertainty in the NO_3 and N_2O_5 mixing ratios and the uncertainty in K_2 at 285 K (factor of 1.3). The red line is the CLD measurement of NO_2. There is good agreement

between the measured and calculated NO_2 mixing ratios on this night, with the major features in NO_2 around midnight, when variations between 0.5 and 3 ppb are nicely captured.

From expression (2), a plot of the product of the NO_2 and NO_3 mixing ratios versus the N_2O_5 mixing ratio should be a straight line with the slope equal to K_2. Such a plot is shown (Fig. 6) for the same dataset (night 8–9 June, 01:00–03:00, $NO_3 > 7$ ppt). The measured NO_2 mixing ratio was converted to a concentration so that the slope is an equilibrium constant in the usual units of inverse concentration (cm^3 molecule^{-1}). The temperature for each $NO_3/N_2O_5/NO_2$ datapoint varied from ∼284 to 287 K during the night (see colour scale). Even though the difference between maximum and minimum temperature was only ∼3 K, it is apparent that the data points obtained at the coolest temperatures result in the largest slope (largest values of K_2), reflecting the strong temperature dependence in K_2. The solid black lines represent the expected slopes at the extremes of the small temperature range covered, and should therefore encompass all the data. The dotted black lines use the values of K_2 at the outer bounds of the recommended uncertainty in this parameter. Essentially all of the data is encompassed by the dotted lines. The relevant temperature for calculating the equilibrium constant is not necessarily that at the inlet, but that experienced by the air mass during the last ∼100 s (approximate relaxation time to equilibrium for the conditions at the Kleiner Feldberg) prior to entering the inlet. As our temperatures are those measured by the German weather service station ∼20 m distant from our inlet this represents a source of uncertainty in our calculations. In this context, the night-time temperatures reported by the local environmental agency (HLUG) are ∼0.5 °C lower than reported by the DWD.

Nonetheless, by selecting data within small temperature windows we were able to derive values of $K_2=1.95\times10^{-10}$ cm^3 molecule^{-1} (284 > T > 283 K, average temperature 284.3 K) and $K_2=1.44\times10^{-10}$ cm^3 at molecule^{-1} (287 > T > 286 average temperature 286.8 K) with a proportional fit to the data. The uncertainty associated with these values of K_2 derived from the field data are related to uncertainty in the NO_3, N_2O_5 and NO_2 measurements, which propagate to a value of ∼23%. and, more significantly, are impacted by the unknown temperature history of the air mass directly before sampling (see above). The statistical errors associated with the fit were less than 1%.

The values of K_2 listed above are in very close agreement (within 2%) with recent measurements made in the field using simultaneous detection of NO_2, NO_3 and N_2O_5 (Osthoff et al., 2007). They also agree (within 7%) with literature evaluations (Sander et al., 2003) of 1.89 and 1.35×10^{-10} cm^3 molecule^{-1} at these respective temperatures. We note that a later evaluation by the same panel and using the same database (Sander et al., 2006) results in slightly worse, but, given the uncertainties involved, acceptable, agreement.
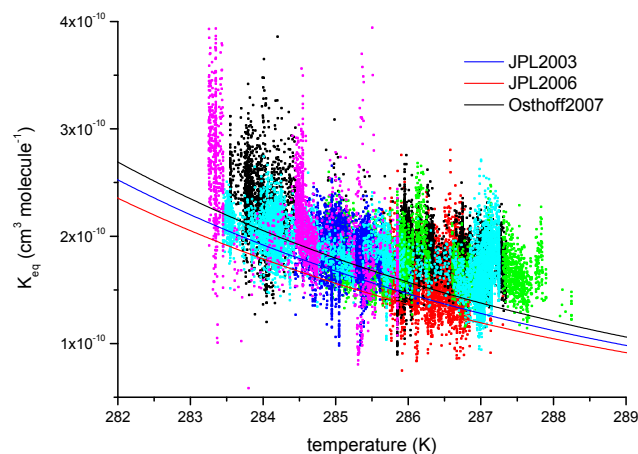
Fig. 7. Determination of the equilibrium constant, K_2 throughout the campaign plotted versus temperature. Data were selected so that NO_3 was always greater than 5 ppt. The red and blue solid lines are recommended values for K_2 from evaluations of laboratory data. The black line is taken from the analysis of Osthoff et al. (2007), based on their field measurements. Different colours are data from different days. JPL2003 = Sander et al. (2003), JPL2006 = Sander et al. (2006), Osthoff2007 = Osthoff et al. (2007).

In Fig. 7, we present equilibrium constants calculated from measured mixing ratios of NO_2, NO_3 and N_2O_5 for each night of the campaign. To avoid systematic error at low mixing ratios, data were selected so that the NO_3 mixing ratio was always greater than 5 ppt.

The temperature dependent values of K_2 thus calculated are compared with evaluations (JPL, 2003, 2006) and recent field determinations (Osthoff et al., 2007). Despite significant scatter in the data is it apparent that, even when neglecting the 30% overall error in our measurements of NO_3 and N_2O_5, the calculated values of K_2 are consistent with the recommended values, with slightly better agreement with the field data of Osthoff et al. (2007).

To date, there have been only a few simultaneous measurements of NO_2, NO_3 and N_2O_5. Our data at the Kleiner Feldberg support observations (Brown et al., 2003b; Aldener et al., 2006; Osthoff et al., 2007) that thermal equilibrium exists at night between these three trace gases under most conditions, the possible exception being at low temperatures. Our data may also be considered to provide confirmation of the laboratory derived equilibrium constant K_2, which has usually been obtained by measuring individual rate constants for the forward and backward processes (Reactions R2a and R2b) via pseudo first-order analysis rather than measurement of equilibrium concentrations, which is difficult to achieve in laboratory set-ups with reactive surfaces. The notable exception to this being the work of Osthoff et al. (2007), in a well characterised, multi-channel cavity apparatus, whose laboratory derived equilibrium constants agree very well with ours (within 6%).

Conversely, assuming that the laboratory derived equilibrium constant is accurately known, we can conclude that our two-channel set-up for NO_3 and N_2O_5 (used for the first time in this campaign) and the associated data correction procedure can accurately measure ambient NO_3 and N_2O_5 mixing ratios. Poor agreement between calculated NO_2 concentrations (via NO_3, N_2O_5 and K_2) and those measured directly were however occasionally observed. This occurred when NO_3 was reactively lost at an aged Teflon filter, resulting in falsification of the N_2O_5/NO_3 ratio and subsequent over-estimation of the NO_2 concentration. Although small, post filter-change discontinuities in the NO_3 signals were usually concealed by their large variability, they were clearly evident in the calculated NO_2 mixing ratio as short term variability in NO_3 and N_2O_5 were closely matched and thus cancelled. Evidence for NO_3 filter loss was seen in the dataset from the 9th–10th when filter changes were performed only every two hours. Similarly, on one night (13–14 May) the high-volume flow inlet was replaced by a 3/8″ PFA tube of ∼550 cm length. This resulted in a ∼30% increase in the calculated, equilibrium amount of NO_2 over a period when NO_2 was actually stable, indicating that ∼30% of the NO_3 had been lost in the inlet. Note that the residence time in the 550 cm length of tubing was ∼0.9 s. Loss of ∼30% of the NO_3 is thus broadly consistent with the loss rate coefficient of 0.25 s^{-1} in PFA tubing reported in the experimental section.

3.2 NO_3 and N_2O_5 lifetimes and loss rates

The NO_3 turnover lifetime (see Eq. 3) at the Taunus Observatory was highly variable with maximum values of ∼1500 s. Generally, the NO_3 lifetime was longest after ∼03:00 following a slow increase from dusk. This is most apparent (Fig. 8) on the nights of the 9th, 12th and 13th, in which the lifetime directly after dusk (at ∼20:00) remained under ∼200 s for the next ∼3 h. Figure 8 also shows the instantaneous NO_3 production (k_1 [NO_2][O_3]) rates during each night (red lines), which were typically between 100 and 300 ppt/h and fairly constant but with some excursions to larger values due to influxes of NO_2.

Recall that the NO_3 lifetime is determined by both direct losses (e.g. gas-phase reaction with biogenic organics) and indirect loss processes involving N_2O_5. The slow increase in NO_3 lifetime after dusk may thus have been due to either a decrease in gas-phase reactivity after dusk or due to a decrease in surface area or reactivity of aerosol. As the NO levels were reduced to below the detection limit in just a few minutes after dusk, the slow rate of build up of NO_3 and N_2O_5 was not due to a reduction in its concentration during this period. Alternatively, an increase in lifetime could also be related to a stabilisation of the lower atmosphere by adiabatic cooling, which would reduce turbulence and thus dry deposition rates. However, the observation on most nights

of the campaign of a clear increase in wind speed following sunset, does not support this possibility.

Before examining aspects of the NO_3 lifetime in more detail it is worthwhile establishing whether a stationary state analysis was applicable for this dataset. Stationary state is formally achieved when the rate of change of NO_3 and N_2O_5 are zero, i.e. $dNO_3/dt=k_1[NO_2][O_3]+k_{-2}[N_2O_5]-k_2[NO_2][O_3]-f_{dir}$ (NO_3)[NO_3]=0 and $dN_2O_5/dt=k_2[NO_2][NO_3]-k_{-2}[N_2O_5]$ $-(f_{het}+f_{homo})[N_2O_5]=0$. The approximate time to acquire stationary state thus depends on the production and loss rates of both NO_3 and N_2O_5.

Time dependent values of dNO_3/dt and dN_2O_5/dt were determined by numerical simulation in a manner similar to that described by Brown et al. (2003a). Input parameters to the simulations were the measured NO_2 and O_3 concentrations and temperature dependent kinetic expressions for Reactions (R1), (R2) (together defining the production rates of NO_3 and N_2O_5) and variable first order loss terms for removal of NO_3 and N_2O_5. The first-order loss terms for NO_3 and N_2O_5 ($f_{dir}(NO_3)$, f_{het}, f_{homo}) were adjusted until the simulated NO_3 and N_2O_5 mixing ratios were similar to those measured. In conjunction with NO_3 and N_2O_5 lifetimes of the order of minutes, the relatively warm night-time temperatures and low NO_2 concentrations at the Kleiner Feldberg in May, meant that stationary state was achieved within 1–2 h after dusk. Given the distance to local emission regions (see above) and wind speeds of between 10 and 20 km/h this suggest that a steady state analysis was appropriate.

The slow increase in NO_3 lifetime early in the night could have been caused by a reduction in the mixing ratio of biogenic trace gases in the hours following dusk. Using rate coefficients of 7.0×10^{-13} and 6.2×10^{-12} cm^3 molecule^{-1} s^{-1} for reaction of NO_3 with isoprene and α-pinene, respectively (IUPAC, 2009) and initially ignoring indirect loss processes, we calculate that a NO_3 lifetime of ∼100 s would be associated with isoprene levels of 0.60 ppb or α-pinene levels of ∼68 ppt. Emissions of biogenic organics are temperature and light-intensity dependent (Fehsenfeld et al., 1992) and the levels mentioned above would appear reasonable for moderate, spring-time emissions of biogenic organics in a forested area.

As we did not take measurements of organic compounds during the campaign we have no data which confirm efficient removal of NO_3 by e.g. isoprene or α-pinene. There appear to be no published datasets on measurements of gas-phase biogenic trace gases at the Kleiner Feldberg, though some data taken with a proton transfer mass spectrometer over a 4 day period in June of 2005 confirmed the expected presence of isoprene and terpenes in this forested area (V. Sinha and J. Williams, personal communication, 2009). Furthermore, these datasets indicate that both isoprene and terpene concentrations decreased slowly after sundown, only returning to baseline levels in the early hours of the next morning.
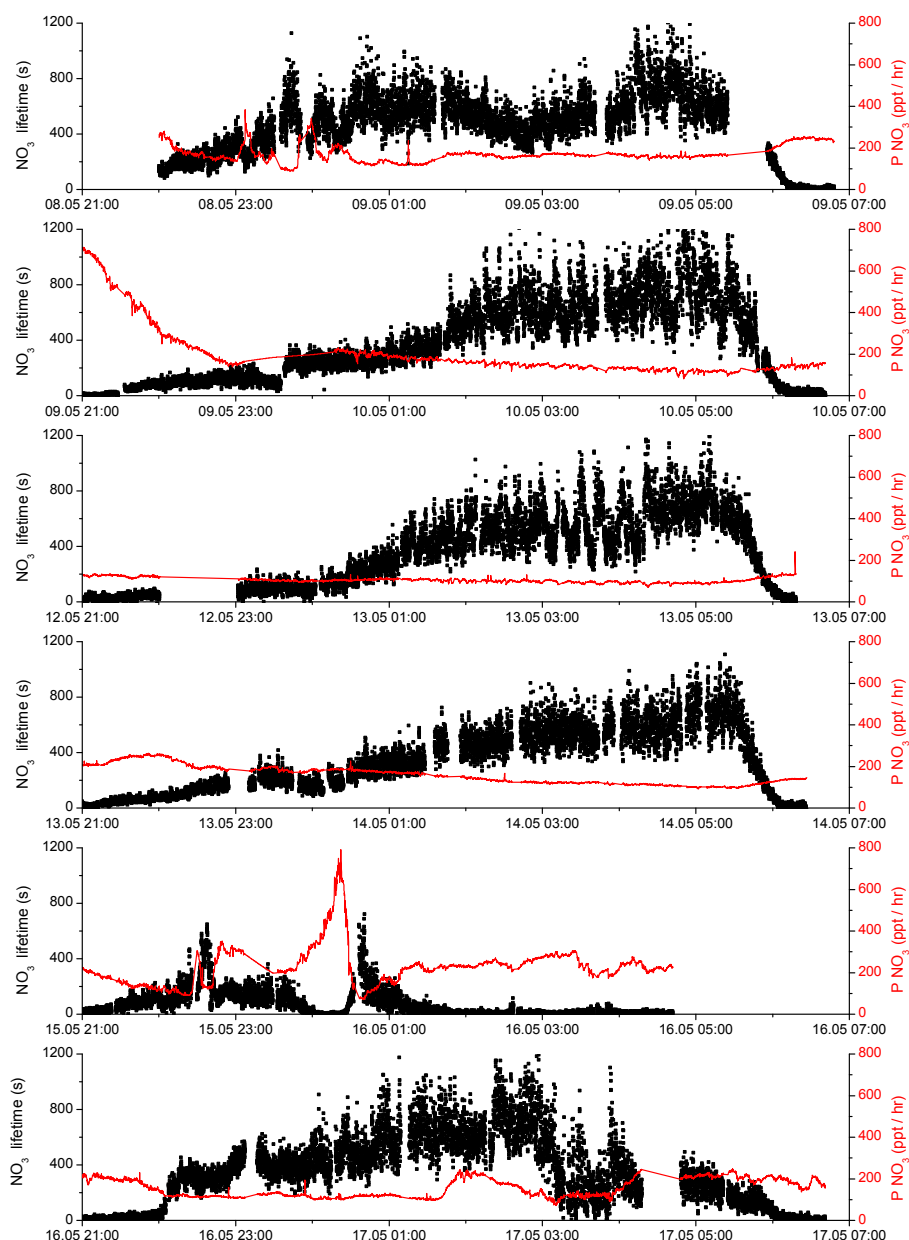
Fig. 8. NO_3 turn-over lifetimes and production rates (red lines) on each night of the campaign.

This observation is thus consistent with the observed slow increase in NO_3 lifetimes over the same period.

A further indication for the presence of biogenic volatile organic compounds (VOCs) is the observation of new particle formation at the Kleiner Feldberg; indeed April–May was the most intense nucleation period during 2008. New particle formation took place during the measurement period on the following days: 8–13 and 15 May (day-time events) as well as during the evening of the 7 and 14 May (night-time events). Temperatures were moderately high and the nocturnal boundary layer rather shallow to facilitate accumulation of emitted VOCs. From the 15th onward the relative

humidity increased substantially causing drizzle or rain and prevented the occurrence of nucleation. During this time the vegetation experienced reduced drought stress resulting (presumably) in lower emission rates. At the same time aerosol mass and surface area declined because of wash out from the atmosphere. In the absence of simultaneous measurements of biogenics or other reactive traces gases (e.g. unsaturated hydrocarbons) that could react with NO_3, the above discussion about the main NO_3 loss reactions remains speculative.

On the last two days of the campaign, the NO_3 lifetime did not show a slow increase to a maximum value, but had already reached $\sim$300–400 s by 23:00 h (Fig. 8). As shown in

Fig. 3, the last two days were meteorologically distinct from the first 4 as the wind direction changed to southwest, bringing cloud cover, lower temperatures and later in the night, rain and fog. The longer lifetime of NO_3 early on these nights was presumably related to reduced biogenic emissions. The periodic strong reductions in lifetime on the night 15–16 May was coincident with precipitation at the site, presumably resulting in loss of N_2O_5 on large droplets (not monitored as the aerosol cut off was $\sim0.5\,\mu m$) or deposition to moist surfaces. Further, indirect processes leading to a reduction in the NO_3 lifetime are the loss of N_2O_5 on aerosol surface and with H_2O vapour. By inverting expression (3) we obtain:

$$f_{ss}(NO_3) \approx f_{dir} + K_{eq}[NO_2](f_{het} + f_{homo}) \qquad (11)$$

The relative importance of direct (gas-phase) and indirect (gas-phase and heterogeneous) losses of NO_3 are displayed for the nights of 13 and 16 May in Fig. 9. The heterogeneous loss rate of N_2O_5 (f_{het}) was calculated from the measured aerosol surface area using expression (4) and scaled by $K_2[NO_2]$ and is presented in Fig. 9 (blue line). The value used for the uptake coefficient, γ, was 0.01, which is within the very large range of values derived from field observations. For example, low values of 0.5–6×10^{-3} have been reported by Brown et al. (2009) in aircraft measurements over Texas, which are consistent with $\sim3\times10^{-3}$ reported by Allan et al. (1999); Ambrose et al. (2007) in marine air masses but much lower than values of 0.02–0.03 (Aldener et al., 2006; Ambrose et al., 2007) also obtained in marine environments. The uptake coefficient used is also smaller by a factor ~3 than measured for loss of N_2O_5 to dilute H_2SO_4 aerosol in the laboratory (Hallquist et al., 2000), though further laboratory studies have shown that the presence of organics can reduce this number significantly (Folkers et al., 2003). Although no aerosol composition data is available, some indication for the type of aerosol encountered at the Taunus Observatory was obtained by observing loss of NO_3 on an aged Teflon filter. In this case, an increase in NO_3 mixing ratio was seen directly after a filter change but was not accompanied by an increase in N_2O_5. This implies that the aerosol gathered on the filter contained a large organic fraction providing a reactive surface for NO_3 but one that did not support efficient hydrolysis of N_2O_5. On the 13 May, it is clear from Fig. 9 that heterogeneous loss of N_2O_5 would have contributed only insignificantly to NO_3 removal even if $\gamma=0.03$ had been used in the calculation. A similar picture emerges for the other nights before the 15th when the wind direction was predominantly Easterly and daytime temperatures were highest. In this period, the calculated maximum NO_3 loss rates due to heterogeneous loss of N_2O_5 were between 1.5 and $6\times10^{-4}\,s^{-1}$ at the end of the night when the NO_3 lifetime was longest. Even then, the heterogeneous loss of N_2O_5 contributed between only 7 and 28%. When averaged over the whole night, this number becomes insignificantly small.
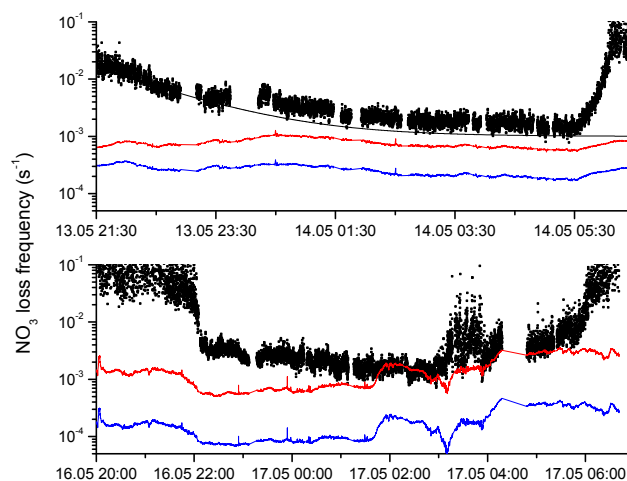
Fig. 9. Measured NO_3 turnover loss frequencies (black datapoints) and calculated loss frequencies due to direct and indirect loss processes on two different nights. Grey line (upper panel only): Hypothetical (direct) loss of NO_3 due to reaction with VOC. Blue line: Indirect loss due to N_2O_5 uptake to aerosol ($f_{het}K_2[NO_2]$). Red line: Indirect loss due to reaction of N_2O_5 with water vapour ($f_{homo}K_2[NO_2]$).

The frequency of NO_3 loss from stationary state caused by the homogeneous reaction of N_2O_5 with water vapour ($f_{homo}K_2[NO_2]$) was initially calculated using the rate coefficients (k_{7a} and k_{7b}) preferred by IUPAC (Atkinson et al., 2004), with H_2O vapour concentrations calculated from the RH and temperature/pressure measurements of the DWD. The loss of NO_3 via this indirect route contributes to its overall loss only later in the night when the overall reactivity of the air has decreased.

Note that the indirect losses of NO_3 via homogeneous and heterogeneous N_2O_5 reactions are constrained by measurements of H_2O vapour and aerosol surface area which do not show a significant trend during the night. Unless the aerosol composition changes greatly during the night (being initially much more reactive than defined by the uptake coefficient above and subsequently becoming increasingly less reactive towards N_2O_5), indirect losses are unlikely to have caused the reduction in reactivity (factor of 10) observed after dusk. In order to reproduce the time dependence of the NO_3 turnover lifetime on the night 12–13 May, $f_{dir}(NO_3)$ was calculated for an initial total reactivity (at dusk) equal to about 200 ppt α-pinene equivalents, which was reduced during the night to ~10 ppt (at 03:00) in a quasi-exponential manner, thus increasing the lifetime from $\sim50\,s$ at 21:00 on 13 May to $\sim1000\,s$ at 03:00 the next morning (grey line, Fig. 9).

For the night 16–17 May a slightly different picture emerges. On this night the NO_3 turn-over lifetime was longer, a result of a decrease in the concentration of VOC and aerosol surface area following a rainy period. Under these

conditions and with an increase in RH to close to 100% the reaction of N_2O_5 with H_2O gains importance and, at 02:00 on the 17th would account for the entire reactivity of the NO_3/N_2O_5 system, i.e. $f_{homo}K_2[NO_2] \sim (\tau ss(NO_3))^{-1}$ if the IUPAC values were used.

The NO_3 losses can be separated into direct and indirect routes by using the fact that the NO_3 turnover lifetime depends non-linearly on the NO_2 concentration if N_2O_5 losses are significant. This is apparent from expression (3), which has been utilised previously to extract e.g. the N_2O_5 hydrolysis contribution to NO_3 loss (Heintz et al., 1996; Geyer et al., 2001; Aldener et al., 2006; Brown et al., 2006, 2009). Plotting the inverse of the NO_3 life-time versus $K_2[NO_2]$ (with $[NO_2]$ in units of molecule cm^{-3}) should give a straight line with slope equal to the N_2O_5 loss rate constant, $f_{indir}(NO_3)$ and intercept equal to the NO_3 loss rate constant $f_{dir}(NO_3)$. This analysis requires selection of data in which $f_{dir}(NO_3)$ and $f_{indir}(NO_3)$ are relatively constant, but for which there is sufficient variation in NO_2 to separate the direct and indirect NO_3 loss terms. On most nights this analysis resulted in strongly curved plots due to the slowly changing lifetime of NO_3 due to reaction with biogenic organics (see above). By selection of a small portion of the data (01:00 to 03:00) on the night of the 16–17 May in which significant variation on NO_2 was observed, a linear relationship was obtained (Fig. 10) with a slope ($f_{indir}(NO_3)$) very close to zero $(5 \pm 5 \times 10^{-6}$ s$^{-1})$ and intercept of $f_{dir}(NO_3) = 1.6 \times 10^{-3}$ s^{-1} (red line). Setting N_2O_5 loss to aerosol to zero ($f_{het}=0$), we take the literature data for k_{7a} and k_{7b} and the water vapour concentration of 2.8×10^{17} molecule cm^{-3} to calculate a value of $f_{homo}=2 \times 10^{-4}$ s^{-1} for this period. As shown in Fig. 10 (black line), this value clearly overestimates the true contribution of indirect losses by at least a factor of 3–4. Reaction (R7b) dominated the homogeneous gas-phase loss of N_2O_5 during the whole campaign with the ratio $k_{7b}[H_2O]^2/k_{7a}[H_2O]$ as large as $\sim$2.5 at RH=100%. Reaction (R7a) is more important only when RH was less than $\sim$30%.

This analysis has thus far ignored loss of N_2O_5 (or NO_3) by dry deposition. Aldener et al. (2006) used a N_2O_5 deposition velocity (V_{dep}) of 1 cm s^{-1} to calculate the contribution of dry deposition to the total loss of N_2O_5. This value was based on estimates for HNO_3 and is not necessarily accurate. Adopting the same value and assuming a boundary layer height of 100 m would result in a frequency for dry deposition of N_2O_5 of 1×10^{-4} s^{-1}, which when multiplied by $k_2[NO_2]$ (usually close to 10) would result in a significant fraction of NO_3 loss throughout the campaign. There are however many uncertainties associated with this calculation as neither the true value of V_{dep} nor the boundary layer height are known. In addition this calculation ignores the strong vertical stratification often seen in the nocturnal boundary layer (Brown et al., 2007). The true factor by which k_7 is overestimated is thus most probably larger than 3–4 as N_2O_5 loss by dry deposition would serve to increase it further. One
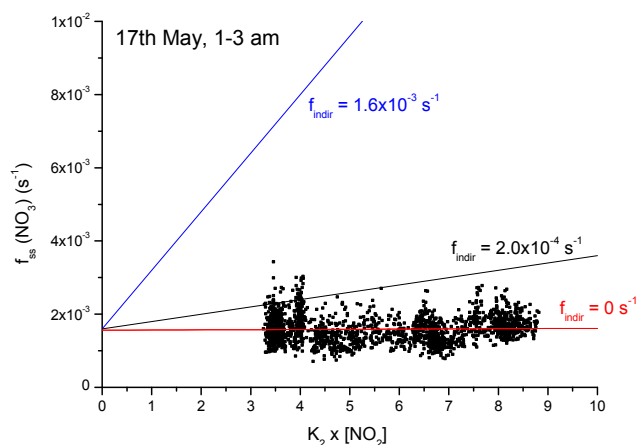
Fig. 10. Separation of direct and indirect loss of NO_3 on the night 16–17 May. The red solid line is the fitted value indicating close to zero indirect loss of NO_3. The black line was obtained by setting heterogeneous N_2O_5 loss to zero and accounting only for reaction with water vapour. The blue line represents equivalency of the direct and indirect losses of NO_3 (intercept = slope = 1.6×10^{-3} s^{-1}). The difference in slope between this and the red line serves to indicate the dominance of direct loss over indirect loss.

caveat to this approach is, however, the assumption that there is no correlation between NO_2 mixing ratios and the major sink process(es) for NO_3 and N_2O_5, which is difficult to prove. The result is however consistent with the conclusions of Brown et al. (2006, 2009), who used airborne measurements of NO_3 and N_2O_5 to indicate that k_7 may be up to a factor 10 smaller than derived from laboratory data.

The blue line in Fig. 10 is the slope expected for equivalent direct and indirect losses of NO_3 and indicates that, for this limited dataset, N_2O_5 destruction plays only a minor role in controlling the NO_3 lifetime. This conclusion is broadly consistent with other measurements at continental, forested sites in Germany, where NO_3 has been found to be removed mainly by reaction with monoterpenes emitted by coniferous trees (Geyer and Platt, 2002).

3.3 NO$_x$ partitioning and daytime versus night-time loss of NO$_x$

The conversion of NO_2 to NO_3 and N_2O_5 followed by reactive losses either with gas-phase species or with aerosols and other surfaces represents a conversion of gas-phase NO_x trace gases to NO_z in both gas and particle phases. In the absence of NO, the fraction of nitrogen oxides (F), which is present in reactive form (i.e. as NO_3 or N_2O_5) at night can be simply expressed as:

$$F = \frac{[NO_3] + 2[N_2O_5]}{[NO_3] + 2[N_2O_5] + [NO_2]} \qquad (12)$$

This expression ignores longer lived NO_x reservoir species such as HNO_3, PAN or halogenated nitrogen oxides, which,
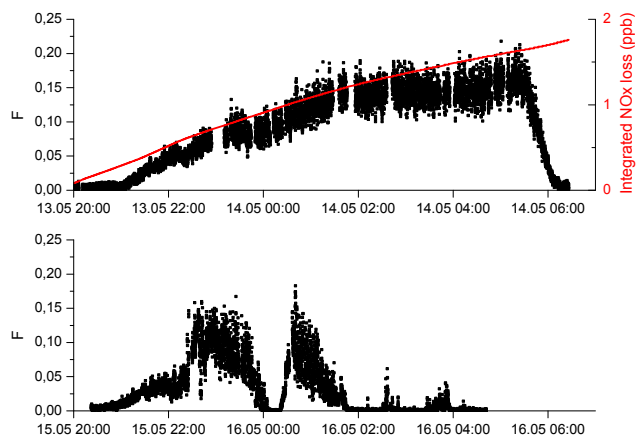
Fig. 11. Fraction (F) of night-time NO_x as NO_3 and N_2O_5 on two meteorologically distinct campaign nights. 13th–14th: warm preceding day and wind from the east. 15th–16th: Wind from the southeast accompanied by rain. The solid red line is the integrated NO_x loss during the night 13–14 May.

unlike NO_3 and N_2O_5 are not in rapid equilibrium with NO_2. The contribution of NO_3 and N_2O_5 to NO_y (which would include trace gases such as HNO_3 and PAN) is, of course smaller.

The partitioning of NO_x to NO_3 and N_2O_5 is favoured by large O_3 concentrations (which increases the NO_2 oxidation rate) and low losses of NO_3 and N_2O_5. Figure 11 displays the variation of F on the nights of 13 and 15 May. The amount of reactive nocturnal nitrogen oxides partitioned as NO_3 and N_2O_5 is initially negligible as the NO_3 and N_2O_5 lifetimes are short. Only later do NO_3 and N_2O_5 reach appreciable concentrations, with F reaching a maximum value of $\sim$20% on 13 and $\sim$15% on 15 May. The slow build up to larger values of F is due to the small rate coefficient for NO_2+O_3 ($\sim$$2\times10^{-17}$ cm^3 molecule^{-1} s^{-1} at 295 K) resulting in NO_2 half lives in the order of hours at 70 ppb O_3 and also due to a slow decline in reactivity of NO_3 in the early part of the night.

The integrated loss of NO_2 (calculated from the NO_2 and O_3 concentrations and the rate coefficient k_1) is also displayed for the night of 13–14 May in this figure. By the end of the night, about 1.5 ppb of NO_2 have been converted via NO_3 and N_2O_5 to gas-phase and particle phase products.

NO_3 and N_2O_5 remaining at the end of the night are rapidly converted photolytically/thermally back to NO_2 (and, less importantly, NO) at dawn, hence the rapid reduction in F at circa 06:00 on the 14th. On this particular night the nocturnal mean value of F was $\sim$9%. The same value was obtained as average over all nights of the campaign on which there was no precipitation. The average value of F was only $\sim$3% on the night 15th–16th, presumably due to efficient loss of N_2O_5 on aqueous surfaces. As the lifetimes of NO_3 and N_2O_5 were much shorter than the duration of the night, and

only a small fraction of NO_2 that has been converted to NO_3 and N_2O_5 is converted back to NO_2 at dawn, we can assume that all NO_2 which was oxidised by O_3 at night represents an irreversible loss of NO_x to either organic or inorganic nitrates. In this case, the loss rate of NO_x (L_{NOx}) is given by:

$$L_{NOx} \approx n \cdot k_1[NO_2][O_3] \tag{13}$$

where the factor n is 1 if NO_3 is lost only directly (e.g. by reaction with VOC) and is 2 if NO_3 is lost indirectly via N_2O_5 formation and reaction as two NO_2 are required to make each N_2O_5 molecule. For the present campaign we have shown that NO_3 is lost predominantly by direct routes, so that n should be close to 1.

The daytime loss of NO_x is dominated by reaction of NO_2 with the OH radical

$$OH + NO_2 \rightarrow HNO_3 \tag{R8}$$

with the rate of loss of NO_2 via this route approximately given by $k_8[OH][NO_2]$, which is also the production rate of HNO_3. At the pressure and temperatures prevalent during the campaign, k_8 has a value of $\sim$$1\times10^{-11}$ cm^3 molecule^{-1} s^{-1}. There appears to be only one set of measurements HNO_3 mixing ratios at the Taunus Observatory, in which values of $\sim$0.1–1 ppb were reported in November of 1990 (Fuzzi et al., 1994).

As no OH measurements were made during the campaign, its concentration was calculated using the parameterisation of Ehhalt and Rohrer (2000). Approximate, time dependent values of J_{NO2} were calculated from the measured global radiation using the parameterisation of Trebs et al. (2009). J_{01D} was calculated from J_{NO2} using relative (solar zenith angle dependent) values taken from the 4.1 version of the NCAR-TUV model (http://cprm.acd.ucar.edu/Models/TUV/Interactive_TUV/). Maximum peak values for J_{01D} and J_{NO2} thus derived were 4×10^{-5} s^{-1} and 9×10^{-3} s^{-1}, respectively, which resulted in peak OH concentrations of $>1\times10^7$ molecule cm^{-3} during the early part of the campaign, decreasing to $\sim$$5\times10^6$ molecule cm^{-3} during the last days of the campaign when insolation was reduced by clouds. The present measurements of relatively large O_3 mixing ratios and previous measurements of peroxy radical mixing ratios of several 10s of pptv in June in previous years at the site (Handisides, 2001) indicate an active photochemistry and imply that these OH concentrations are reasonable. They are also consistent with daytime measurements of OH at another forested mountain site under very similar levels of insolation and with comparable levels of O_3 (Handisides et al., 2003).

Figure 12 displays calculated rates of NO_2 loss (in ppb/hour) via both reaction with OH and with O_3. during a period of 7 days of the campaign. Night-time losses via reaction of NO_2+O_3 are calculated only when global radiation was less than 20 W m^{-2} and NO_2 photolysis should be insignificant. At the beginning of the campaign, when insolation was high, daytime NO_2 losses (0.2–1 ppb per hour)
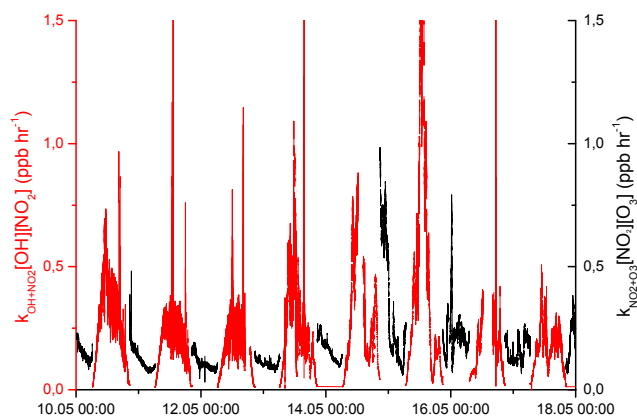
Fig. 12. Daytime (k_{OH+NO2}[OH][NO$_2$], in red) versus night-time (k_{O3+NO2}[O$_3$][NO$_2$], in black) loss rates (ppb/h) of NO$_x$ at the Taunus Observatorium in May 2008.

dominated (by a factor of $\sim$2–3) over night-time losses. This picture changes for the last days of the campaign, where day and night-time losses were approximately equal at about 0.2 ppb per hour. The simple calculations above show that, at the surface, day- and night-time losses of NO$_x$ are similar. However, as the ratio of night-time to day-time losses depends on insolation at the site, night-time losses will be favoured still more in the colder months as O$_3$ photolysis and OH production rate drop significantly. The fact that the night-time boundary layer is shallower than in the daytime will however have the converse effect and favour daytime oxidation. We can conclude that night-time loss of NO$_x$ due to NO$_3$ (and N$_2$O$_5$) formation is comparable to daytime loss driven by OH at the Taunus Observatory, confirming speculation that nitrate driven acidity in cloud water at the Kleiner Feldberg could be caused either by HNO$_3$ or N$_2$O$_5$ uptake (Fuzzi et al., 1994). As vertical profiles of NO$_2$/O$_3$ etc were not measured, our conclusion applies only to the surface.

Although no VOCs were measured during the campaign, the persistently high night-time mixing ratios of NO$_3$ indicate an important role for the oxidation of VOCs at the site. An average daytime OH concentrations of $\sim$4$\times$10^6 molecule cm^{-3} and an average night-time mixing ratio of 10 pptv for NO$_3$ result in a concentration ratio that favours NO$_3$ by a factor of $\sim$60. The ratios of rate coefficients (k_{OH}/k_{NO3}) for reaction of OH and NO$_3$ with isoprene and several monoterpenes favour OH and may be calculated from reviewed kinetic data (Atkinson and Arey, 2003) as: isoprene (147), α-pinene (8.5), limonene (13.4), sabinene (11.7). These numbers indicate that whereas NO$_3$ will contribute significantly to isoprene removal, it would dominate for the mono-terpenes listed above. The simple calculation does not take the diurnal changes in VOC emission rates mixing ratios into account and a more detailed understanding of the relative importance of daytime versus night-time removal of boundary layer NO$_x$ and the fate of reactive VOCs at this

site would require diel measurements of both the major oxidants (OH and NO$_3$) and the VOCs.

4 Conclusions

A complete set of nocturnal nitrogen oxides, O$_3$ and aerosol surface area was measured for the first time at the Taunus Observatory. The measurements provided both a test of the new NO$_3$/N$_2$O$_5$ instrument and delivered valuable information concerning night-time oxidation at the site. Both NO$_3$ and N$_2$O$_5$ were present above the detection limits on all nights and the relative concentrations were in accord with the temperature, NO$_2$ and the equilibrium constant for N$_2$O$_5$ formation and thermal dissociation. The major sink of NO$_x$ was inferred to be direct loss of NO$_3$ by reaction with biogenic hydrocarbons and nocturnal chemistry at this site was shown to contribute significantly both to the conversion of NO$_x$ to NO$_y$ and likely to the oxidation of biogenic VOCs. A steady state analysis was used to estimate direct and indirect losses of NO$_3$ and N$_2$O$_5$ and revealed shortcomings in the laboratory derived kinetics of the reaction of N$_2$O$_5$ with water-vapour.

References

Aldener, M., Brown, S. S., Stark, H., Williams, E. J., Lerner, B. M., Kuster, W. C., Goldan, P. D., Quinn, P. K., Bates, T. S., Fehsenfeld, F. C., and Ravishankara, A. R.: Reactivity and loss mechanisms of NO$_3$ and N$_2$O$_5$ in a polluted marine environment: Results from in situ measurements during New England Air Quality Study 2002, J. Geophys. Res., 111, D23S73, doi:10.1029/2006JD007252, 2006.

Allan, B. J., Carslaw, N., Coe, H., Burgess, R. A., and Plane, J. M. C.: Observations of the nitrate radical in the marine boundary layer, J. Atmos. Chem., 33, 129–154, 1999.

Allan, B. J., McFiggans, G., Plane, J. M. C., Coe, H., and McFadyen, G. G.: The nitrate radical in the remote marine boundary layer, J. Geophys. Res., 105, 24191–24204, 2000.

Ambrose, J. L., Mao, H., Mayne, H. R., Stutz, J., Talbot, R., and Sive, B. C.: Night-time nitrate radical chemistry at Appledore island, Maine during the 2004 international consortium for atmospheric research on transport and transformation, J. Geophys. Res., 112, D21302, doi:101.1029/2007JD008756, 2007.

Apodaca, R. L., Simpson, W. R., Brauers, T., Brown, S. S., Cohen, R. C., Crowley, J., Dorn, H. P., Dubé, W. P., Fry, J., Fuchs, H., Haseler, R., Heitmann, U., Kato, S., Kajii, Y., Kiendler-Scharr, A., Labazan, I., Matsumoto, J., Nishida, S., Tillmann, R., Rohrer, F., Rollings, A.W., Schlosser, E., Schuster, G., Tillmann, R., Wahner, A., Wegener, R., and Wooldridge, P. J.: Intercomparison of N_2O_5 sensors using the SAPHIR reaction chamber, Atmos. Chem. Phys. Discusss., in preparation, 2010.

Atkinson, R. and Arey, J.: Atmospheric degradation of volatile organic compounds, Chem. Rev., 103, 4605–4638, 2003.

Atkinson, R., Baulch, D. L., Cox, R. A., Crowley, J. N., Hampson, R. F., Hynes, R. G., Jenkin, M. E., Rossi, M. J., and Troe, J.: Evaluated kinetic and photochemical data for atmospheric chemistry: Volume I – gas phase reactions of O_x, HO_x, NO_x and SO_x species, Atmos. Chem. Phys., 4, 1461–1738, 2004, http://www.atmos-chem-phys.net/4/1461/2004/.

Berden, G., Peeters, R., and Meijer, G.: Cavity ring-down spectroscopy: Experimental schemes and applications, Int. Rev. Phys. Chem., 19, 565–607, 2000.

Brown, S. S., Dube, W. P., Fuchs, H., Ryerson, T. B., Wollny, A. G., Brock, C. A., Bahreini, R., Middlebrook, A. M., Neuman, J. A., Atlas, E., Roberts, J. M., Osthoff, H. D., Trainer, M., Fehsenfeld, F. C., and Ravishankara, A. R.: Reactive uptake coefficients for N_2O_5 determined from aircraft measurements during the Second Texas Air Quality Study: Comparison to current model parameterizations, J. Geophys. Res., 114, D00F10, doi:10.1029/2008JD011679, 2009.

Brown, S. S., Dubé, W. P., Osthoff, H. D., Wolfe, D. E., Angevine, W. M., and Ravishankara, A. R.: High resolution vertical distributions of NO_3 and N_2O_5 through the nocturnal boundary layer, Atmos. Chem. Phys., 7, 139–149, 2007, http://www.atmos-chem-phys.net/7/139/2007/.

Brown, S. S., Ryerson, T. B., Wollny, A. G., Brock, C. A., Peltier, R., Sullivan, A. P., Weber, R. J., Dube, W. P., Trainer, M., Meagher, J. F., Fehsenfeld, F. C., and Ravishankara, A. R.: Variability in nocturnal nitrogen oxide processing and its role in regional air quality, Science, 311, 67–70, 2006.

Brown, S. S., Stark, H., and Ravishankara, A. R.: Applicability of the steady state approximation to the interpretation of atmospheric observations of NO_3 and N_2O_5, J. Geophys. Res., 108, 4539, doi:10.1029/2003JD003407, 2003a.

Brown, S. S., Stark, H., Ryerson, T. B., Williams, E. J., Nicks, D. K., Trainer, M., Fehsenfeld, F. C., and Ravishankara, A. R.: Nitrogen oxides in the nocturnal boundary layer: Simultaneous in situ measurements of NO_3, N_2O_5, NO_2, NO, and O_3, J. Geophys. Res., 108, 4299, doi:10.1029/2002JD002917, 2003b.

Curtis, A. R. and Sweetenham, W. P.: Facsimile, AERE, Report R-12805, 1987.

Dorn, H. P., Apodaca, R. L., Ball, S. M., Brauers, T., Brown, S. S., Crowley, J. N., Dube, W. P., Fuchs, H., Häseler, R., Heitmann, U., Jones, R. L., Labazan, I., Langridge, J., Meinen, J., Platt, U., Pöhler, D., Rohrer, F., Ruth, A. A., Schlosser, E., Schuster, G., Shillings, A., Simpson, W., Thieser, J., Varma, R., Venables, D., and Wahner, A.: Intercomparison of NO_3 radical detection instruments in the Atmosphere Simulation Chamber SAPHIR., Atmos. Chem. Phys. Discuss., in preparation, 2010.

Ehhalt, D. H. and Rohrer, F.: Dependence of the OH concentration on solar UV, J. Geophys. Res., 105, 3565–3571, 2000.

Fehsenfeld, F., Calvert, J., Fall, R., Goldan, P., Guenther, A., He-

witt, C.N., Lamb, B., Liu, S., Trainer, M., Westberg, H., and Zimmerman, P.: Emissions of volatile organic compounds from vegetation and the implications for atmospheric chemistry, Global Biogeochem. Cycles, 6, 389–430, 1992.

Folkers, M., Mentel, T. F., and Wahner, A.: Influence of an organic coating on the reactivity of aqueous aerosols probed by the heterogeneous hydrolysis of N_2O_5, Geophys. Res. Lett., 30, 1644, doi:10.1029/2003GL017168, 2003.

Fontijn, A., Sabadell, A. J., and Ronco, R. J.: Homogeneous chemiluminescent measurement of nitric oxide with ozone – Implications for continuous selective monitoring of gaseous air pollutants, Anal. Chem., 42, 575–579, 1970.

Fuzzi, S., Facchini, M. C., Schell, D., Wobrock, W., Winkler, P., Arends, B. G., Kessel, M., Mols, J. J., Pahl, S., Schneider, T., Berner, A., Solly, I., Kruisz, C., Kalina, M., Fierlinger, H., Hallberg, A., Vitali, P., Santoli, L., and Tigli, G.: Multiphase Chemistry and Acidity of Clouds at Kleiner-Feldberg, J. Atmos. Chem., 19, 87–106, 1994.

Geyer, A., Alicke, B., Konrad, S., Schmitz, T., Stutz, J., and Platt, U.: Chemistry and oxidation capacity of the nitrate radical in the continental boundary layer near Berlin, J. Geophys. Res., 106, 8013–8025, 2001.

Geyer, A. and Platt, U.: Temperature dependence of the NO_3 loss frequency: A new indicator for the contribution of NO_3 to the oxidation of monoterpenes and NO_x removal in the atmosphere, J. Geophys. Res., 107, 4431, doi:10.1029/2001JD001215, 2002.

Hallquist, M., Stewart, D. J., Baker, J., and Cox, R. A.: Hydrolysis of N_2O_5 on submicron sulfuric acid aerosols, J. Phys. Chem. A, 104, 3984–3990, 2000.

Handisides, G. M.: The influence of peroxy radicals on ozone production, PhD thesis, Johann Wolfgang Goethe Universität, Fachbereich Geowissenschaften, Frankfurt am Main, 2001.

Handisides, G. M., Plass-Dlmer, C., Gilge, S., Bingemer, H., and Berresheim, H.: Hohenpeissenberg Photochemical Experiment (HOPE 2000): Measurements and photostationary state calculations of OH and peroxy radicals, Atmos. Chem. Phys., 3, 1565–1588, 2003, http://www.atmos-chem-phys.net/3/1565/2003/.

Heintz, F., Platt, U., Flentje, H., and Dubois, R.: Long-term observation of nitrate radicals at the tor station, Kap Arkona (Rugen), J. Geophys. Res., 101, 22891–22910, 1996.

IUPAC, Subcommittee for gas kinetic data evaluation (Ammann, M., Atkinson, R., Cox, R. A., Crowley, J. N., Hynes, R. G., Jenkin, M. E., Mellouki, W., Rossi, M. J., Troe, J., and Wallington, T. J.): Evaluated kinetic data: http://www.iupac-kinetic.ch.cam.ac.uk/, 2009.

Kley, D. and McFarland, M.: Chemiluminescence detector for NO and NO_2, Atmos. Technol., 12, 63–69, 1980.

Kraus, A. and Hofzumahaus, A.: Field measurements of atmospheric photolysis frequencies for O_3, NO_2, HCHO, CH_3CHO, hooh, and HONO by UV spectroradiometry, J. Atmos. Chem. 31, 161–180, 1998.

Mazurenka, M., Orr-Ewing, A. J., Peverall, R., and Ritchie, G. A. D.: Cavity ring-down and cavity enhanced spectroscopy using diode lasers, Annu. Rep. Prog. Chem., Sect C, 101, 100–142, 2005.

Orphal, J., Fellows, C. E., and Flaud, P. M.: The visible absorption spectrum of NO_3 measured by high-resolution Fourier transform spectroscopy, J. Geophys. Res., 108, 4077,

doi:10.1029/2002JD002489, 2003.

Osthoff, H. D., Pilling, M. J., Ravishankara, A. R., and Brown, S. S.: Temperature dependence of the NO_3 absorption cross-section above 298 K and determination of the equilibrium constant for $NO_3 + NO_2 < - > N_2O_5$ at atmospherically relevant conditions, Phys. Chem. Chem. Phys., 9, 5785–5793, 2007.

Ridley, B. A., Grahek, F. E., and Walega, J. G.: A small, high-sensitivity, medium-response ozone detector suitable for measurements from light aircraft, J. Atmos. Ocean. Technol., 9, 142–148, 1992.

Sander, S. P., Friedl, R. R., Golden, D. M., Kurylo, M. J., Huie, R. E., Orkin, V. L., Moortgat, G. K., Ravishankara, A. R., Kolb, C. E., Molina, M. J., and Finlayson-Pitts, B. J.: Chemical Kinetics and Photochemical Data for Use in Atmospheric Studies, Evaluation Number 14, Jet Propulsion Laboratory, National Aeronautics ans Space Administration/Jet Propulsion Laboratory/California Institute of Technology, Pasadena, CA, 2003.

Sander, S. P., Friedl, R. R., Golden, D. M., Kurylo, M. J., Huie, R. E., Orkin, V. L., Moortgat, G. K., Ravishankara, A. R., Kolb, C. E., Molina, M. J., and Finlayson-Pitts, B. J.: Chemical kinetics and photochemical data for use in atmospheric studies: Evaluation Number 15, Jet Propulsion Laboratory, National Aeronautics and Space Administration/Jet Propulsion Laboratory/California Institute of Technology, Pasadena, CA, 2006.

Schuster, G., Labazan, I., and Crowley, J. N.: A cavity ring down/cavity enhanced absorption device for measurement of ambient NO_3 and N_2O_5, Atmos. Meas. Tech., 2, 1–13, 2009, http://www.atmos-meas-tech.net/2/1/2009/.

Trebs, I., Bohn, B., Ammann, C., Rummel, U., Blumthaler, M., Königstedt, R., Meixner, F. X., Fan, S., and Andreae, M. O.: Relationship between the NO_2 photolysis frequency and the solar global irradiance, Atmos. Meas. Tech., 2, 725–739, 2009, http://www.atmos-meas-tech.net/2/725/2009/.

Wayne, R. P., Barnes, I., Biggs, P., Burrows, J. P., Canosa-Mas, C. E., Hjorth, J., Le Bras, G., Moortgat, G. K., Perner, D., Poulet, G., Restelli, G., and Sidebottom, H.: The nitrate radical: Physics, chemistry, and the atmosphere, Atmos. Environ., 25A, 1–206, 1991.

Wetter, T.: Eine Untersuchung zur Charakterisierung der Zeitlichen Variabilität det luftchemischen Bedingungen am Taunus-Observatorium: Messungen des CO und H_2 Mischverhältnises im Winter 1996/7, Johan Wolfgang Goethe-Universität, Fachbereich Geowissenschaft, Frankfurt am Main, 1998.

Yokelson, R. J., Burkholder, J. B., Fox, R. W., Talukdar, R. K., and Ravishankara, A. R.: Temperature-dependence of the NO_3 absorption-Spectrum, J. Phys. Chem., 98, 13144–13150, 1994.